

Analysis of a Single Squared Wingsail Design as an Auxiliary Propulsion System on a Tanker Ship

*Hilman Ikmalul Iman*¹, *Ahmad Nasirudin*¹, *Hesty Anita Kurniawati*¹, *Wasis Dwi Aryawan*¹, *Hasanudin*¹, *Erzad Iskandar Putra*¹, and *Ardi Nugroho Yulianto*¹

¹Department of Naval Architecture, Faculty of Marine Technology, Institut Teknologi Sepuluh Nopember (ITS), Surabaya, Indonesia

Abstract. This study presents an analysis of a single squared wingsail used as an auxiliary propulsion system for an 8,700 DWT oil tanker. The objective is to evaluate the aerodynamic performance and stability feasibility of the wingsail and to assess its contribution to engine power reduction. Numerical simulations were conducted to obtain lift and drag coefficients for three aspect ratios (AR 2, 4, and 6) with a constant sail area of 289 m². Stability assessment was performed at multiple voyage waypoints along the Gresik–Bontang round trip using the weather criterion ($K \geq 1$) and metacentric height ($GM \geq 0.3$ m). The results indicate that all configurations satisfy the stability requirements, while AR 4 provides the most effective performance in terms of thrust generation and power reduction. The AR 4 configuration, with a span of 34.0 m and a chord of 8.5 m, achieves the highest average engine power reduction of 5.3%, compared to 4.9% for AR 2 and 4.1% for AR 6. These findings demonstrate that the selected wingsail configuration is aerodynamically effective and stable, offering a practical solution for auxiliary wind-assisted propulsion on tanker vessels.

1 Introduction

Climate change has become one of the most critical challenges facing humanity, influencing almost every aspect of the environment and human activity. Its effects are increasingly visible through extreme temperature variations, rising sea levels, more frequent floods and droughts, powerful storms, wildfires, landslides, and the accelerated melting of polar ice caps [1,2]. Recognizing the seriousness of this global issue, the United Nations (UN) established the Intergovernmental Panel on Climate Change (IPCC) in 1988 to provide comprehensive scientific assessments of climate-related phenomena [3]. This was followed by the establishment of the United Nations Framework Convention on Climate Change (UNFCCC) in 1992, which brought nations together to discuss and coordinate climate policies. Subsequent milestones, such as the Kyoto Protocol in 1997 and the Paris Agreement in 2015, have reinforced international commitments to maintaining global temperature increases below 1.5°C above pre-industrial levels [4].

Within this global framework, the maritime sector plays an essential role in world trade and transportation, serving as an integral component of international supply chains and economic connectivity [5]. Despite its efficiency in moving large volumes of goods, the industry continues to evolve in response to technological and environmental developments. The International Maritime Organization (IMO), through its series of Greenhouse Gas (GHG) Studies, has highlighted the significant contribution of the maritime sector to global emissions. IMO as the global authority on maritime safety and performance standards, has introduced several frameworks to promote the modernization of ship systems and design. The Energy Efficiency Design Index (EEDI) and the Energy Efficiency Existing Ship Index (EEXI) are two key indices established to ensure ships adopt innovative design concepts and operational improvements [6]. These frameworks have encouraged ship designers and researchers to explore the use of advanced technologies that can improve overall vessel performance while maintaining structural and operational safety [7].

One promising approach that has attracted renewed attention is wind-assisted ship propulsion (WASP). The concept of using wind power for marine propulsion has existed for millennia, particularly in the early stages of maritime trade when sails were the primary means of propulsion [8]. In modern times, this concept has evolved with advances in aerodynamic design, control systems, and material technology. The development of modern devices such as Flettner rotors, suction wings, and rigid wingsails has made it possible to utilize wind energy as an auxiliary source of thrust in large ocean-going vessels [9,10]. By generating aerodynamic lift and drag forces, these systems provide additional thrust that can supplement engine-driven propulsion, thereby improving the vessel's hydrodynamic behaviour and potentially reduce engine load.

Among the different types of WASP technologies, the rigid or squared wingsail configuration has shown promise for integration into large ships. Unlike flexible fabric sails, rigid wingsails use airfoil-shaped structures like airplane wings to generate lift more effectively [11]. This configuration allows for higher lift-to-drag ratios, better control of aerodynamic forces, and greater efficiency at a wide range of wind angles. Furthermore, the squared design simplifies

the mechanical system, making it easier to construct, maintain, and retrofit on existing vessels without major modifications to the hull or deck structure. The wingsail can also be automated for deployment and adjustment, which enhances operational safety and consistency under varying weather conditions [12].

However, the installation of a wingsail system introduces several engineering challenges. The aerodynamic forces acting on the sail can induce heeling and overturning moments that alter the ship's hydrostatic balance. These effects become particularly significant in large displacement vessels, where the center of effort of the wingsail is located high above the waterline. Such forces can influence the metacentric height and overall stability of the vessel. Therefore, it is crucial to evaluate the aerodynamic loading in conjunction with the ship's stability criteria to ensure safe and reliable operation under different wind directions and speeds.

2 Method

2.1 Case Study

2.1.1 Main Dimension

The ship selected for this case study is a 8700-ton DWT tanker operating in Indonesia, with the specification as listed in Table 1.

Table 1. Main Dimension

Item	Value
Length Between Perpendiculars (Lpp)	106.4 m
Breadth (B)	18.2 m
Height (H)	10 m
Draught (T)	7.8 m
Volume Displacement (V)	11500 m ³
Service Speed (Vs)	13.5 knots
Engine Power	5310 HP

2.1.2 Ship's Route

In this study, wind data were gathered along the ship's operational route from July 2023 to July 2024, from reference [13,14]. The data include true wind speed and wind direction recorded during the vessel's voyages over a one-year period. These parameters were collected to represent the actual wind conditions experienced by the ship during its operations, serving as input for the aerodynamic and performance analyses of the wingsail.

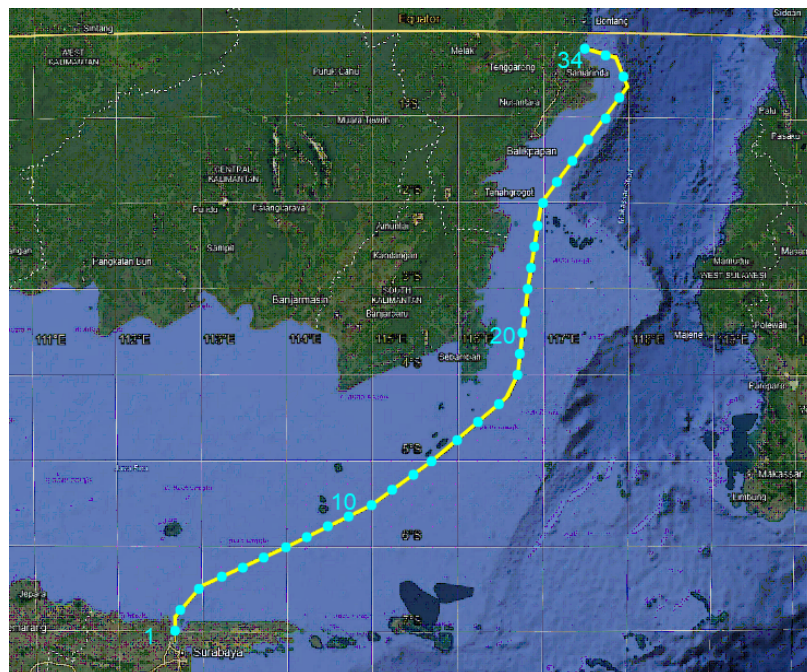


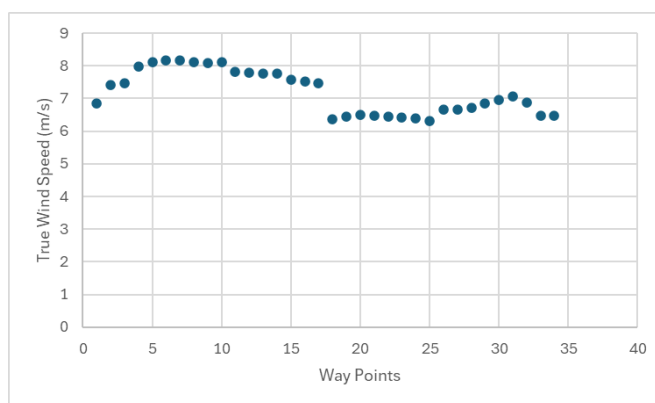
Fig. 1. Ship's operating route and waypoints

The ship operates along a domestic trade route connecting Gresik and Bontang, located in the Java Sea and Makassar Strait. This route represents a typical east-west shipping corridor frequently used by tanker vessels for fuel and chemical transport. The voyage between Gresik and Bontang is conducted regularly in a round-trip pattern, providing consistent environmental conditions suitable for evaluating wind characteristics and potential wingsail performance over the course of one year.

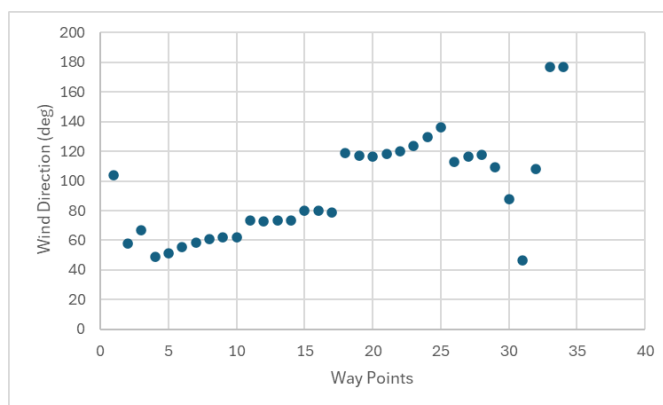
2.1.3 Ship Voyage Data

To analyze the potential performance and applicability of the wingsail system, this study utilized wind data collected along the ship’s operational route for a continuous one-year period, from July 2023 to July 2024. The dataset comprises both wind speed and wind direction information recorded throughout the vessel’s typical voyage path. This data serves as a fundamental input to evaluate the aerodynamic behavior of the wingsail and to estimate its possible contribution under realistic sea conditions.

Fig. 3.(a) illustrates the variation of true wind speed along the route during the observation period. The wind data were recorded at several coordinate points along the voyage. Fig. 2.(b) presents the wind direction. The directional variability suggests that the route experiences a combination of favorable and crosswind conditions, which are essential considerations in estimating the aerodynamic performance and thrust generation of the wingsail. Overall, the wind characteristics within this period represent realistic environmental conditions for analyzing the wingsail’s effectiveness in assisting propulsion and reducing fuel consumption.



(a)



(b)

Fig. 2. Data way points for (a) true wind speed (b) wind direction

Fig. 3 presents the true wind speed and wind direction distributions for the entire observation period. The data show that the average wind speed along the ship’s operational route generally ranges between 6 and 7 knots, with occasional peaks above 8 knots during certain months. These variations indicate that the vessel encounters a wide range of relative wind conditions depending on its heading and seasonal changes in the Indonesian maritime region.

2.2 Wingsail Geometries

In this study, the wingsail employed is a rigid squared sail using the NACA 0012 airfoil profile. The total sail area used in this work is 289 m², selected as the reference area for further performance evaluation. To investigate the influence of aspect ratio on aerodynamic behavior, the sail area is divided into three geometries with aspect ratios (AR) of 2, 4, and 6. For the AR 2 configuration, the sail dimensions consist of a span of 24 m and a chord of 12 m. The AR 4 configuration has a span of 34 m and a chord of 8.5 m, while the AR 6 configuration is defined by a span of 41.6 m and a chord of 6.9 m. These variations allow for comparative analysis of aerodynamic coefficients and performance trends across different geometrical arrangements of the wingsail.

2.2.1 Configuration of Wingsail

In this study, the wingsail employed is a single squared rigid wingsail designed as an auxiliary propulsion device for an 8,700 DWT oil tanker. The wingsail has a rectangular planform with an aspect ratio (AR) of 2, 4, and 6 and a total sail area (A_S) of 289 m². The airfoil section used for the design is based on the NACA 0012 symmetrical profile. The wingsail geometry is selected to achieve an optimal balance between aerodynamic efficiency and stability performance while maintaining structural simplicity for potential retrofit applications. The wingsail is installed at a longitudinal position of 79.5 m from the aft perpendicular (AP), corresponding to a location between the midship section and the forecabin deck. This placement is selected to provide sufficient exposure to incoming wind while maintaining an acceptable longitudinal weight distribution and minimizing adverse effects on the vessel's trim and stability characteristics.

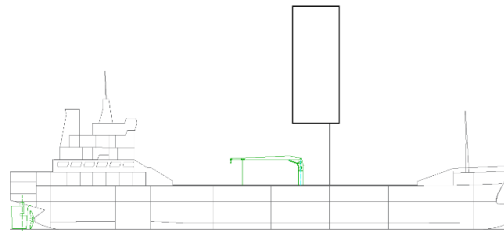


Fig. 3. Wingsail configuration

The rectangular configuration was chosen because of its straightforward manufacturing process and consistent aerodynamic performance across the span. With span length and chord length, the designed wingsail offers sufficient lift generation for thrust assistance without exceeding the vessel's stability limits. The aerodynamic performance parameters, including lift and drag, are evaluated through numerical simulations to determine the effectiveness of the proposed design.

2.3 Simulation Set-Up

The numerical simulations were conducted to evaluate the aerodynamic performance of a squared rigid wingsail for three different aspect ratios, namely AR 2, AR 4, and AR 6. These configurations were selected to represent variations in wingsail geometry while maintaining a constant total sail area of 289 m². The geometrical modifications were applied by adjusting the span and chord dimensions according to the specified aspect ratios, ensuring that only the influence of aspect ratio on aerodynamic behavior was investigated.

Each wingsail model was developed using the NACA 0012 airfoil profile and analyzed under identical operational and environmental conditions. The numerical approach was employed to capture the flow characteristics around the wingsail surface and to determine the corresponding aerodynamic forces generated by each configuration. The primary aerodynamic parameters obtained from the simulations were the lift coefficient (C_l) and drag coefficient (C_d), which were then used as inputs in the subsequent thrust and performance analysis.

This simulation framework enables a consistent comparison between the three aspect ratios, allowing the influence of geometric variation on aerodynamic efficiency to be clearly identified. The results of this analysis provide a reliable basis for selecting the most appropriate wingsail configuration in terms of aerodynamic performance for integration as an auxiliary propulsion system on the tanker vessel.

2.4 Wingsail Thrust Calculations

The forces acting on the sail are illustrated in Fig. 1. The thrust force (T) generated by the sail is the component in ship direction of the resultant force (R) of lift (L) and drag (D). Additionally, the R also produces a side force (S).

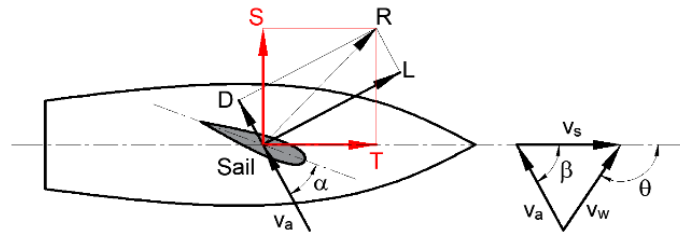


Fig. 4. Sailing vessel forces

L and D are generated by the sail at an angle α relative to the direction of the apparent wind with velocity V_A . The apparent wind velocity V_A is the resultant of the true wind velocity (V_w) and the ship's velocity (V_s). The angle between V_A and V_s is denoted as β , while the angle between V_w and V_s is represented as θ .

T and S can be calculated by using (1) and (2).

$$\mathbf{T} = \mathbf{L} \sin \beta - \mathbf{D} \cos \beta \quad (1)$$

$$\mathbf{S} = \mathbf{L} \cos \beta + \mathbf{D} \sin \beta \quad (2)$$

where,

$$\beta = \arccos [(V_w \cos \theta + V_s) / V_A] \quad (3)$$

$$V_a = (V_w^2 + V_s^2 + 2 V_w V_s \cos \theta)^{0.5} \quad (4)$$

$$\mathbf{L} = 0.5 \rho V_A^2 A_s C_l \quad (5)$$

$$\mathbf{D} = 0.5 \rho V_A^2 A_s C_d \quad (6)$$

In this formulation, C_l and C_d are obtained from the numerical simulations for each wingsail configuration, while A_s represents the sail area and AR denotes the aspect ratio. These parameters are used as fundamental inputs for calculating the aerodynamic forces and thrust generated by the wingsail. The aerodynamic forces acting on the wingsail are governed by the apparent wind velocity (V_A) and the wind angle relative to the ship's course (β). These parameters determine the magnitude of lift (L) and drag (D) generated by the airfoil-shaped sail. The resulting forces are resolved into thrust (T), acting in the longitudinal direction of the ship, and side force (S), acting perpendicular to the ship's motion. While the thrust force contributes directly to reducing the propulsion demand of the main engine, the side force induces heeling moments that affect ship stability. Therefore, the aerodynamic performance of the wingsail must be evaluated in conjunction with stability criteria to ensure that the generated thrust does not compromise the vessel's safety.

2.5 Stability Criteria and Calculations

The stability assessment was conducted to evaluate the influence of the wingsail installation on the vessel's transverse stability. Two main criteria were applied: the weather criterion and the metacentric height (GM) requirement. The weather criterion defines the ratio between the overturning moment generated by the aerodynamic force on wingsail (M_q) and wind heeling moment (M_f). This relationship can be expressed as:

$$K = M_q / M_f \quad (7)$$

The vessel is considered stable when $K \geq 1$, which indicates that the restoring moment is sufficient to counteract the heeling effect produced by the wingsail. The weather criterion, defined as the ratio between the overturning moment (M_q) induced by aerodynamic wind forces and the restoring moment (M_f) provided by the ship, indicates the vessel's ability to resist wind-induced heeling. When K is lower than unity ($K < 1$), the overturning moment exceeds the available restoring moment, implying that the ship may experience excessive heel or be unable to recover to an upright position under wind loading conditions. The overturning moment (M_q) is obtained from the product of the aerodynamic force acting on the sail. The wind heeling moment (M_f) consists of two main components, the moment acting on the sail structure (M_{fs}) and the moment acting on the hull body (M_{fb}). M_q and M_f can be calculated by using (9) and (10).

$$\mathbf{M}_q = l_q \Delta \quad (8)$$

$$\mathbf{M}_f = \mathbf{M}_{fs} + \mathbf{M}_{fb} \quad (9)$$

The second stability criterion involves the metacentric height (GM), which characterizes the ship's initial transverse stability. The vessel should maintain a minimum GM value of 0.3 m to ensure adequate righting capability under

external heeling forces. A GM value below the minimum requirement ($GM < 0.3$ m) indicates insufficient righting leverage, resulting in slow roll response and increased vulnerability to capsizing when subjected to external disturbances. Therefore, both criteria must be satisfied to ensure that the wingsail-generated aerodynamic forces do not compromise the vessel's stability during operation. Both criteria were employed in this study to determine the acceptable wingsail dimensions that maintain compliance with IMO stability requirements.

3 Result and Discussions

3.1 Lift and Drag Coefficient

The lift coefficient (C_l) and drag coefficient (C_d) were obtained from the numerical simulation results for each wingsail configuration with aspect ratios of 2, 4, and 6. These coefficients represent the aerodynamic response of the sail under varying true wind angles along the ship's operational route. The extracted C_l and C_d values are subsequently used as primary inputs in the thrust calculation to evaluate the aerodynamic performance of the wingsail and its contribution to ship propulsion. The variation of these coefficients across different aspect ratios provides a basis for comparing the thrust and performance trend of each wingsail configuration.

A grid independence study was conducted to ensure that the numerical results obtained from the numerical simulations are not significantly influenced by mesh resolution. Several mesh densities were tested by progressively increasing the total number of elements, and the corresponding lift coefficient (C_L) and drag coefficient (C_D) were monitored. As shown in Fig. X, an increase in mesh density leads to noticeable variations in both C_L and C_D at lower element counts; however, beyond approximately 5×10^6 elements, the changes in aerodynamic coefficients become marginal. The lift coefficient shows a gradual convergence trend, while the drag coefficient stabilizes with only negligible differences for finer meshes. This indicates that further mesh refinement does not significantly improve solution accuracy. Therefore, the selected mesh resolution provides a reasonable balance between computational efficiency and numerical accuracy and is considered sufficient for subsequent aerodynamic analyses.

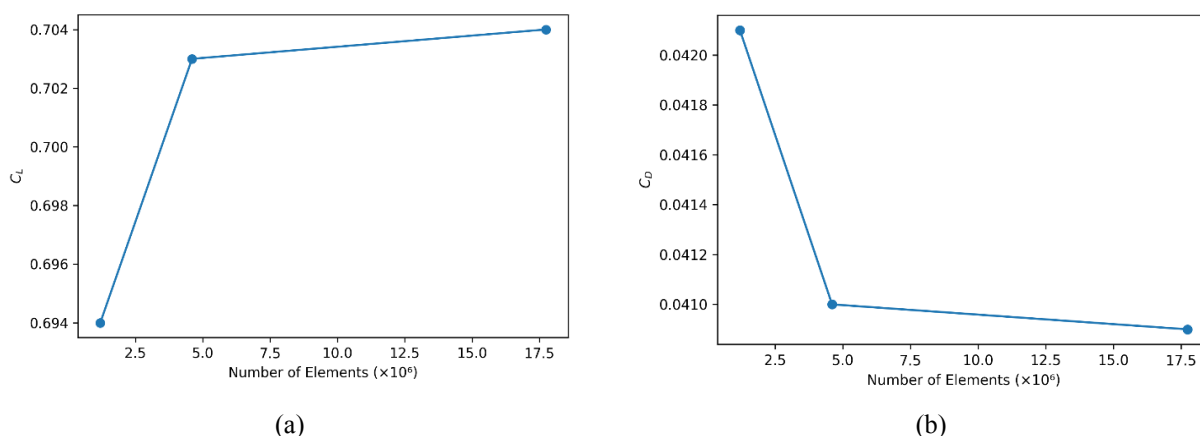


Fig. 5. Grid independence study (a) C_l (b) C_d

The lift coefficient (C_l) and drag coefficient (C_d) were obtained from the numerical simulations for each aspect ratio (AR = 2, 4, and 6) under three Reynolds numbers, namely $Re = 3.3M$, $6.0M$, and $8.9M$. Figures X and Y present the variation of C_l and C_d to aspect ratio, illustrating the aerodynamic response of the squared wingsail geometry.

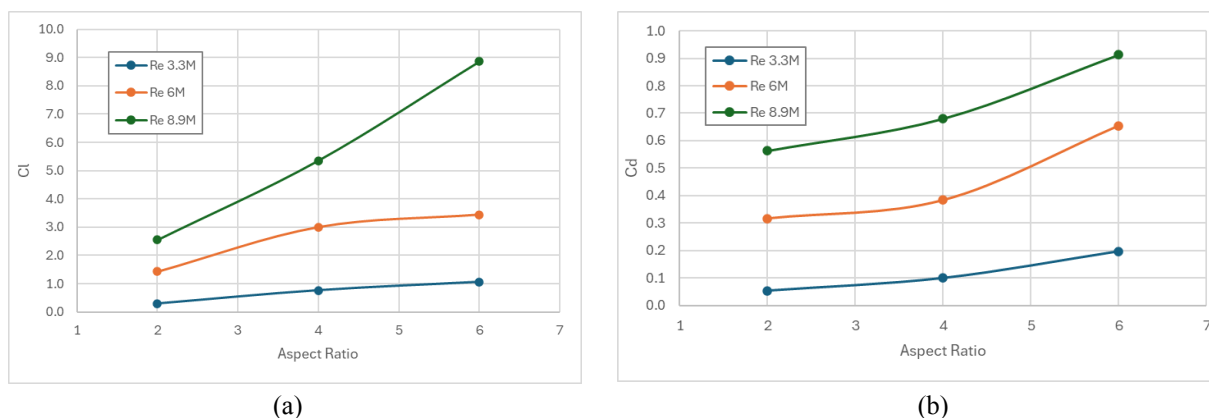


Fig. 6. (a) C_l maximum and (b) C_d maximum for different aspect ratio and reynold number

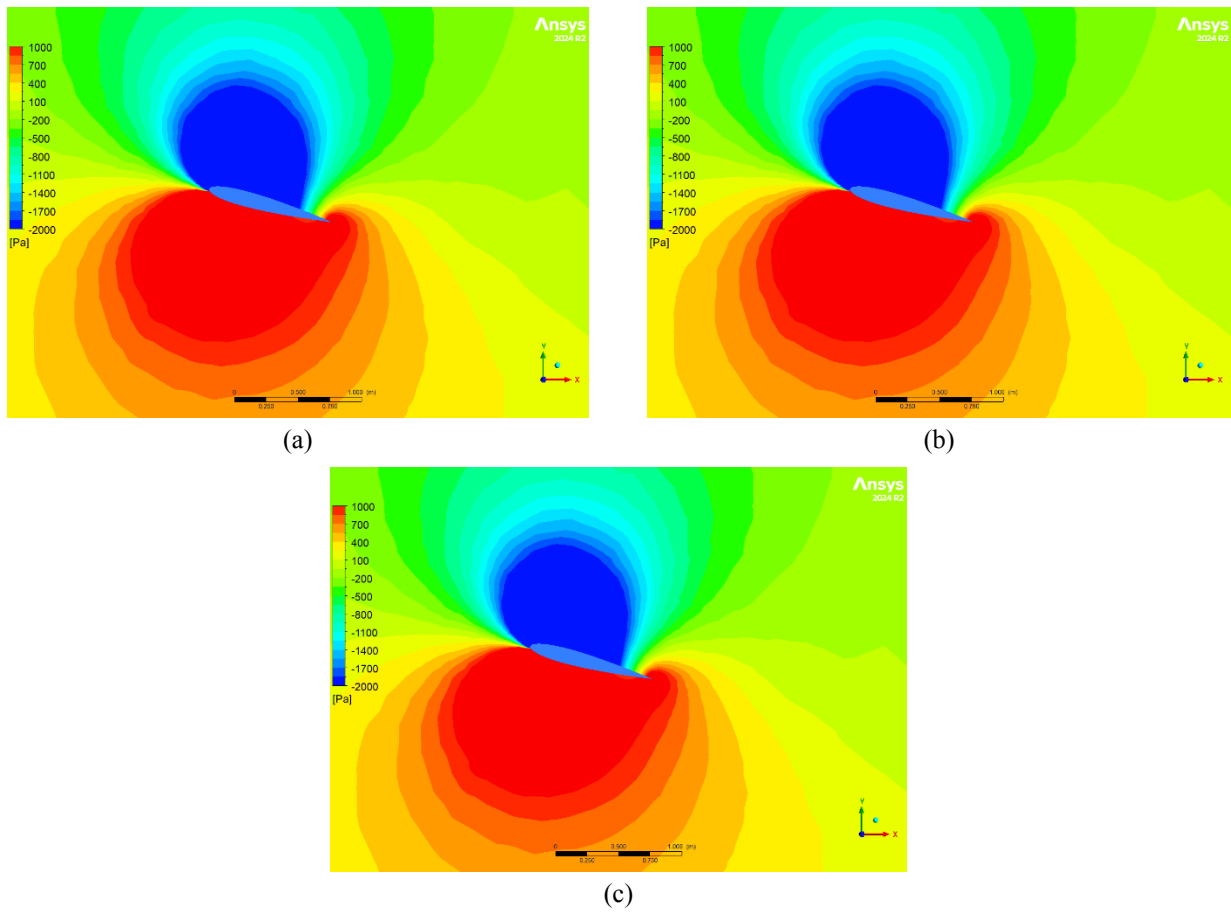


Fig. 7. Contour pressure (a) AR 2 (b) AR 4 (c) AR 6

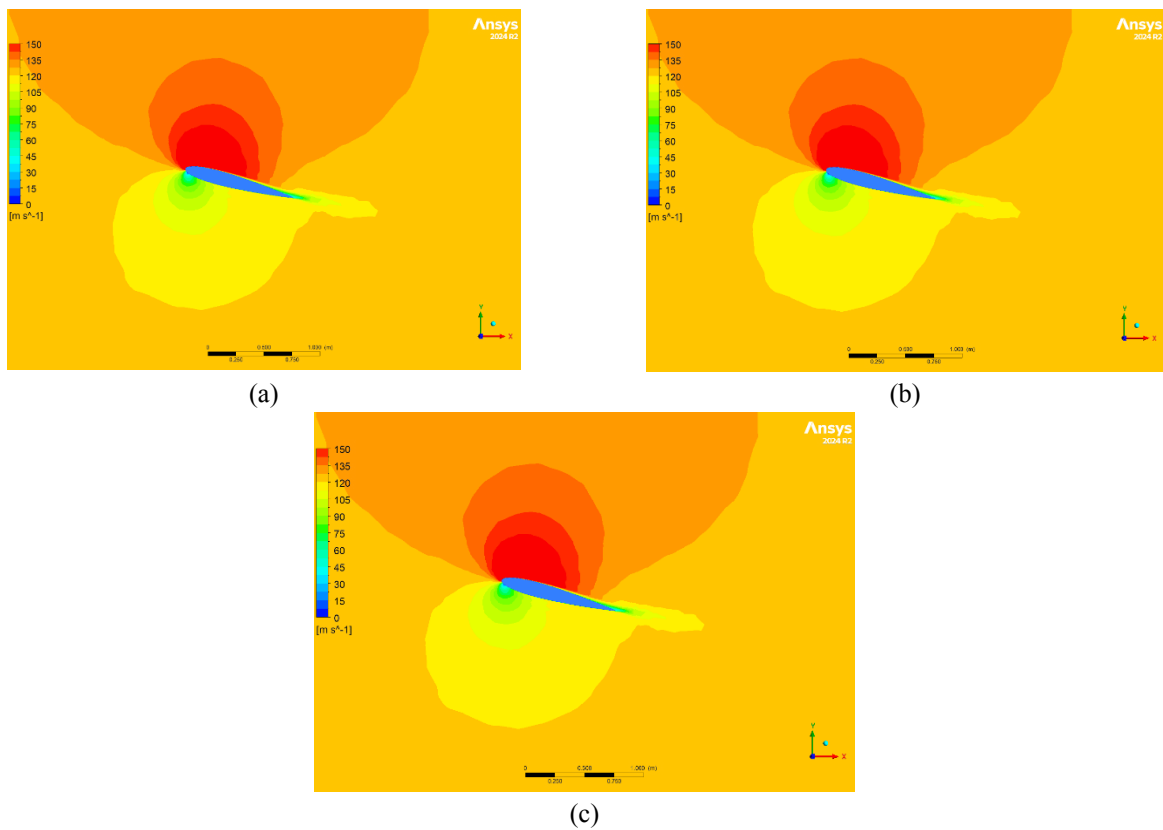


Fig. 8. Contour velocity (a) AR 2 (b) AR 4 (c) AR 6

In Fig. 5, demonstrate that increasing aspect ratio leads to higher lift and drag coefficients across all Reynolds numbers. This trend indicates that while larger aspect ratios enhance lift generation, they also introduce greater aerodynamic resistance.

Based on the results, the AR 4 configuration produced the highest lift coefficient, with a C_l value of 1.50, indicating superior lift generation capability compared to AR 2 and AR 6. The AR 2 configuration yielded a C_l of 1.40, while AR 6 showed the lowest lift coefficient at 1.16. This trend suggests that increasing AR does not always result in higher lift for the squared rigid wingsail, as geometric efficiency and flow behavior also influence aerodynamic performance. In terms of drag, AR 2 exhibited the highest drag coefficient with a C_d value of 0.310, followed by AR 6 with 0.217. The lowest drag coefficient was obtained by the AR 4 configuration at 0.162. This indicates that AR 4 offers a more favorable balance between lift and drag, resulting in a higher lift-to-drag ratio compared to the other configurations.

3.2 Stability Calculations

The stability calculations were conducted to evaluate the effect of the wingsail installation on the ship's overall stability performance. Based on the analysis, the wingsail generates an overturning moment (M_q) and a wind heeling moment (M_f) that were used to determine the stability ratio (K) and the metacentric height (GM).

The stability evaluation was conducted to assess the feasibility of the selected wingsail configuration under realistic operational conditions along the ship's entire voyage route. The route considered in this study consists of 34 waypoints for a single direction, resulting in a total of 68 evaluation points for a complete round trip between Gresik and Bontang. At each waypoint, the stability parameters were calculated based on the prevailing wind conditions and the corresponding aerodynamic forces generated by the wingsail.

Initially, three aspect ratios ($AR = 2, 4, \text{ and } 6$) were examined to investigate their influence on both aerodynamic performance and ship stability. The results indicated that the AR 2 configuration successfully satisfied the stability criteria at all evaluated points, with the weather criterion ratio K remaining above 1 and the metacentric height GM exceeding 0.3 m throughout the entire route. Conversely, the AR 4 configuration failed to meet the stability requirements at several locations, particularly at 34 evaluated points where the K value dropped below the acceptable limit, indicating insufficient restoring capability under certain wind conditions. The AR 6 configuration exhibited an even higher tendency to violate the stability constraints.

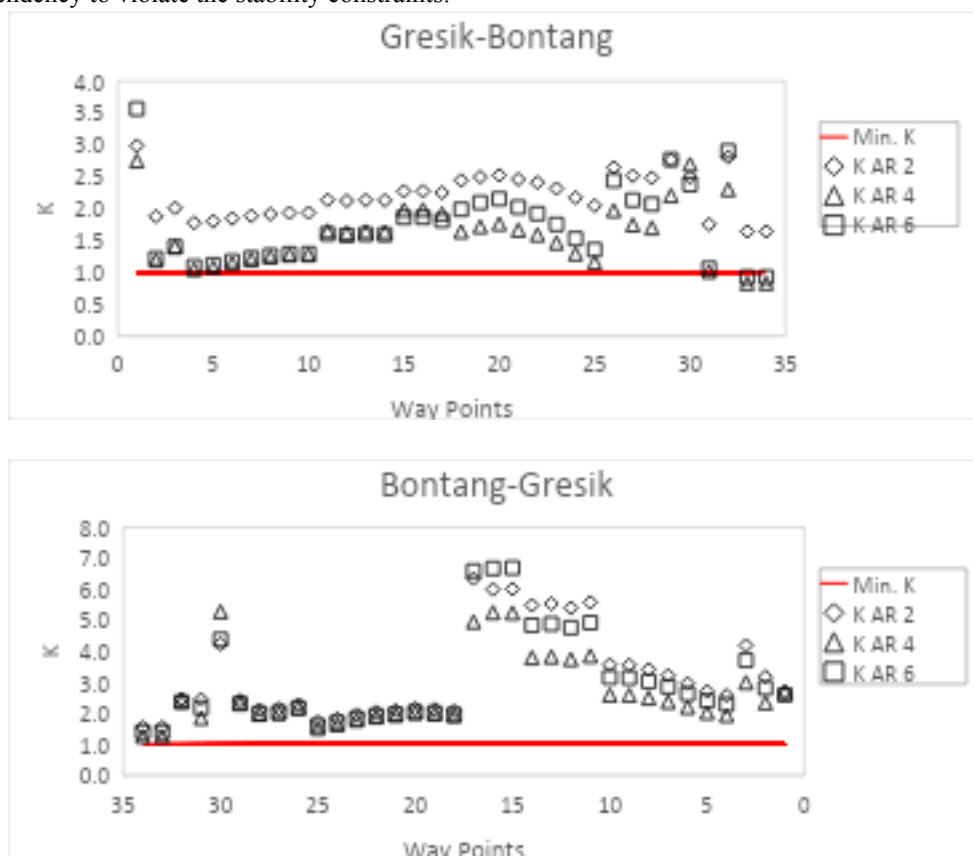


Fig. 9. Weather criterion (K) at each waypoints

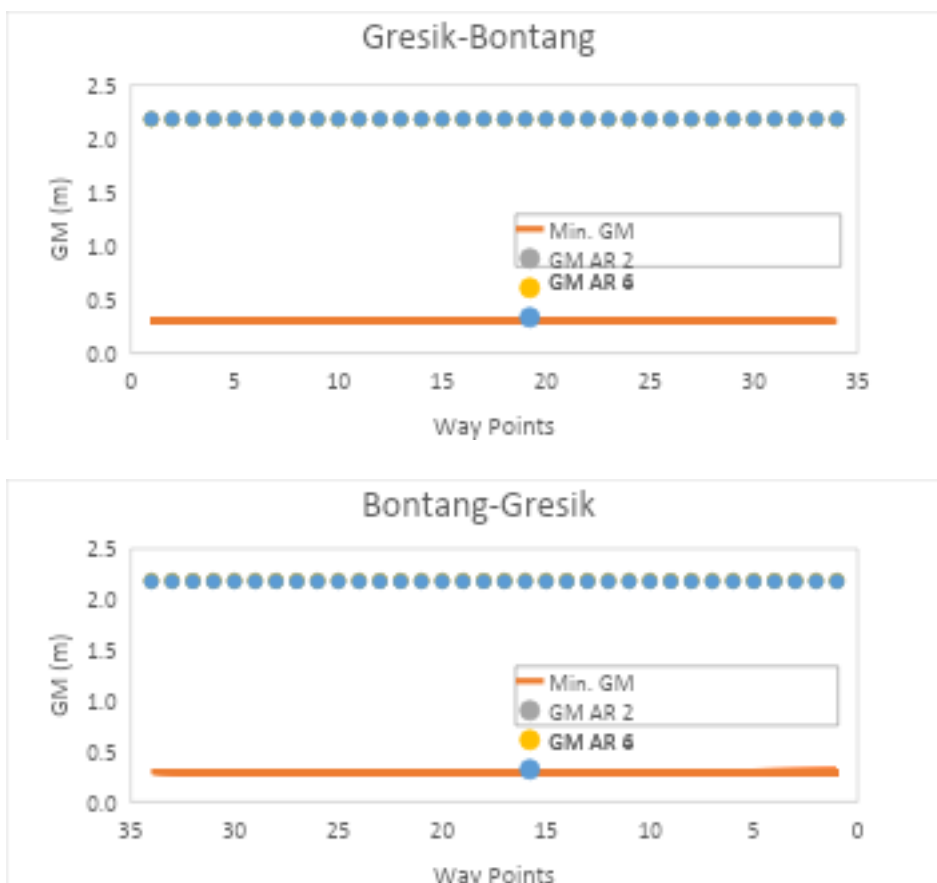


Fig. 10. GM criterion at each waypoints

To balance between aerodynamic performance and stability safety, a compromise aspect ratio of AR 4 was selected as the final configuration. The stability ratio (K) was further evaluated at each waypoint along the ship’s operational route using Equation (7) for the selected wingsail configuration with $AR = 4$. The analysis shows that all calculated K values along the Gresik–Bontang segment satisfy the weather criterion requirement, with values exceeding 1 and reaching up to approximately 4. For the route from Bontang to Gresik, the stability ratio exhibits even higher margins, with peak values approaching 6.3 at specific waypoints. This consistent compliance across all evaluated points confirms that the proposed wingsail configuration provides sufficient restoring capability against wind-induced overturning moments throughout the entire round-trip operation.

The metacentric height (GM) was obtained from stability analysis using Maxsurf Stability to evaluate the effect of the wingsail installation on the vessel’s transverse stability. For the Gresik–Bontang route under ballast condition, the GM values were 2.187 m for AR 2, 2.184 m for AR 4, and 2.180 m for AR 6. Meanwhile, for the Bontang–Gresik route under full load condition, the corresponding GM values were 2.194 m for AR 2, 2.187 m for AR 4, and 2.178 m for AR 6.

3.3 Evaluation of Aspect Ratio and Thrust Performance

The comparative assessment of aspect ratios AR 2, AR 4, and AR 6 were conducted based on both aerodynamic performance and stability compliance along the vessel’s operational route. Although AR 2 demonstrated full compliance with the stability criteria at all evaluated waypoints, its aerodynamic performance, particularly in terms of thrust generation, was comparatively lower due to its reduced effective span. Conversely, AR 4 exhibited improved aerodynamic characteristics; however, stability analysis revealed that this configuration did not satisfy the weather criterion at several waypoints, indicating potential operational limitations under varying wind conditions. Considering these findings, an intermediate aspect ratio of AR 4 was adopted as a compromise configuration, providing a balanced combination of enhanced thrust potential and acceptable stability performance. This selected aspect ratio ensures that the wingsail operates within the required stability limits while achieving higher propulsive contribution compared to AR 2, thereby supporting a more effective integration of the wingsail system as an auxiliary propulsion device.

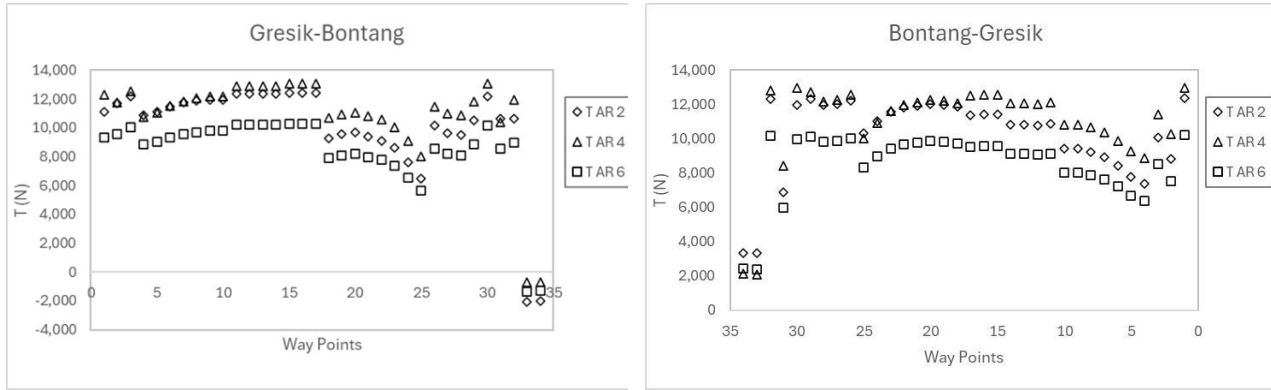


Fig. 11. Wingsail thrust

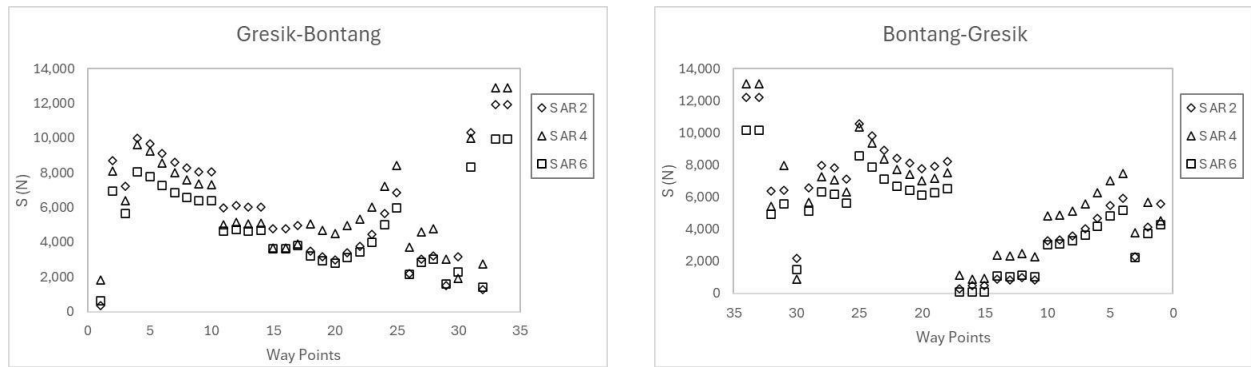


Fig. 12. Wingsail side force

3.4 Contribution of Wingsail

The contribution of the wingsail system to propulsion performance was evaluated by comparing the average aerodynamic thrust generated by the sail with the ship’s resistance at the service speed of 13.5 knots. The analysis was performed separately for each voyage direction to account for differences in wind characteristics and hydrodynamic resistance.

For the Gresik–Bontang voyage, the total ship resistance at the service speed of 13.5 knots was evaluated to be 205.4 kN. Under the corresponding wind conditions along this route, the AR 4 wingsail configuration generated sufficient aerodynamic thrust to achieve an engine power reduction of 5.29%. This reduction indicates that the wingsail effectively assisted the main propulsion system by partially offsetting the hydrodynamic resistance, thereby decreasing the required brake power output while maintaining the vessel’s operational speed.

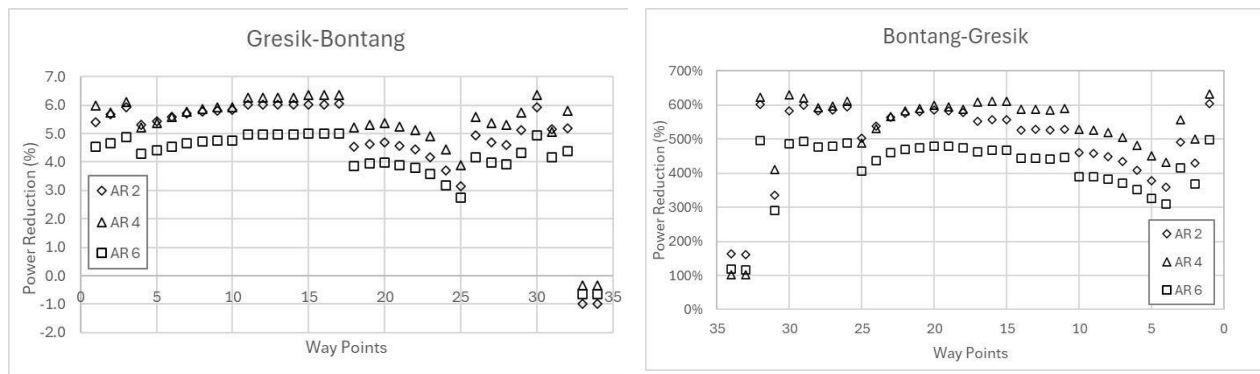


Fig. 13. Power reduction

Similarly, for the Bontang to Gresik, the total ship resistance increased to 229.6 kN due to variations in environmental and operational conditions. Despite the higher resistance, the AR 4 wingsail maintained robust aerodynamic performance, resulting in a slightly greater engine power reduction of 5.34%. The consistency of these power savings across both voyage directions demonstrates the reliability of the wingsail system in providing auxiliary

propulsive contribution under varying wind and resistance conditions. Considering both voyage directions, the overall average engine power reduction provided by the AR 4 wingsail for a complete round trip was therefore determined to be 5.3%, confirming the consistent contribution of the wingsail system in reducing propulsion power demand under varying operational conditions.

4 Conclusions

The results of this study indicate that a wingsail area of 289 m² represents the maximum feasible configuration that fully satisfies the applied stability criteria for all evaluated aspect ratios (AR 2, AR 4, and AR 6). This area defines the upper operational limit at which the wingsail system can be implemented without compromising the vessel's transverse stability and safety margins. Among the investigated configurations, the wingsail with an aspect ratio of 4, corresponding to a span of 34 m and a chord of 8.5 m, demonstrates the most favorable overall performance. This configuration generates the highest average thrust contribution, resulting in an average engine power reduction of approximately 5.3% over the evaluated voyage. The reduction in required engine power is achieved through the longitudinal thrust component produced by aerodynamic lift and drag forces acting on the wingsail, which partially offsets the ship resistance and decreases the propulsion demand of the main engine. Consequently, the AR 4 configuration provides an effective balance between aerodynamic performance and stability compliance and is therefore identified as the optimal design for integration on the selected tanker vessel within the scope of this study. Future research should extend the present analysis by incorporating structural design and strength assessment of the wingsail, evaluating dynamic wind and wave effects, and investigating operational control strategies and alternative placement configurations to further improve propulsion efficiency and ensure reliable performance under realistic operating conditions.

References

- [1] W. I. Okonkwo, “Impacts of Climate Change on Environment and the Remedies @ ECRTD-UK : <https://www.eajournals.org/>,” vol. 8, no. 2, pp. 1–9, 2022.
- [2] E. A. Singh and M. R. Shindikar, “A Comprehensive Review on Climate Change and Its Effects,” vol. 13, no. 11, pp. 924–931, 2023, doi: 10.9734/IJECC/2023/v13i113240
- [3] F. Committee, “Protection of global climate for present and future generations of mankind: Programme budget implications of draft resolution A/C. 2/58/L. 14/Rev. 1: Report of the 5th Committee: General Assembly, 58th session,” no. January 2004, pp. 2004–2005, 2005.
- [4] P. R. S. Masson-Delmotte, V. P. Zhai, H.-O. Pörtner, D. Roberts, J. Skea, M. I. G. A. Pirani, W. Moufouma-Okia, C. Péan, R. Pidcock, S. Connors, J.B.R. Matthews, Y. Chen, X. Zhou, and T. W. E. Lonnoy, T. Maycock, M. Tignor, *IPCC, 2018: Summary for Policymakers. In: Global Warming of 1.5°C. An IPCC Special Report on the impacts of global warming of 1.5°C above pre-industrial levels and related global greenhouse gas emission pathways, in the context of strengthening the global*. Cambridge and New York: Cambridge University Press, 2018. doi: <https://doi.org/10.1017/9781009157940.001>.
- [5] Melnyk Oleksiy Mykolayovych, “STRATEGIES FOR THE DEVELOPMENT OF MARITIME TRANSPORTATION AND METHODS FOR EFFICIENT OPERATION,” vol. 8, no. 22, pp. 324–335, 2023.
- [6] M. Tadros, M. Ventura, and C. G. Soares, “Review of the IMO Initiatives for Ship Energy Efficiency and Their Implications,” pp. 662–680, 2023.
- [7] A. T. A. Wijaya, I. M. Ariana, H. Prastowo, and T. Pitana, “Consideration of Energy Efficiency Operational Index evaluation Consideration of Energy Efficiency Operational Index evaluation”.
- [8] T. Chou, V. Kosmas, M. Acciaro, and K. Renken, “A Comeback of Wind Power in Shipping : An Economic and Operational Review on the Wind-Assisted Ship Propulsion Technology,” 2021.
- [9] G. Atkinson, H. Nguyen, and J. Binns, “Considerations regarding the use of rigid sails on modern powered ships,” *Cogent Eng.*, vol. 5, no. 1, pp. 1–20, 2018, doi: 10.1080/23311916.2018.1543564
- [10] P. F. Rynne, S. Member, and K. D. Von Ellenrieder, “Development and Preliminary Experimental Validation of a Wind- and Solar-Powered Autonomous Surface Vehicle,” *IEEE J. Ocean. Eng.*, vol. 35, no. 4, pp. 971–983, 2010, doi: 10.1109/JOE.2010.2078311
- [11] A. Hillenbrand, A. Oceanbird, and J. Kutteneuler, “Wind Tunnel Tests of a Two-Element Wingsail with Focus on Near-Stall Aerodynamics,” vol. 9, no. 1, pp. 110–127, 2025.
- [12] R. Zhang *et al.*, “Numerical investigation on the effects of heel on the aerodynamic performance of wing sails,” *Ocean Eng.*, vol. 305, no. April, p. 117897, 2024, doi: 10.1016/j.oceaneng.2024.117897. Available: <https://doi.org/10.1016/j.oceaneng.2024.117897>
- [13] “Global Fishing Watch.” Available: <https://globalfishingwatch.org/>. [Accessed: Sep. 20, 2025]
- [14] R. Schlitzer, “Ocean Data View,” 2016. Available: <http://odv.awi.de>. [Accessed: Sep. 20, 2025]